Tellus (1986), *38A*, 462–477

On the determination of vertical structure functions for time-dependent flow problems

By ALAN M. DAVIES, *Institute of Oceanographic Sciences, Bidston Observatory, Birkenhead, Merseyside L43 7RA, UK* and GUNNAR K. FURNES, *Norsk Hydro Research Centre, P.O. Box 4313, N-5001 Bergen, Norway*

(Manuscript received May 13; in final form December 27, 1985)

ABSTRACT

A method of solving the viscous three-dimensional hydrodynamic equations is developed using an expansion of vertical structure functions (modes). Both slip and no-slip bottom boundary conditions can be incorporated in the method. Vertical structure functions for arbitrary vertical variations of viscosity are computed using either the Runge-Kutta-Merson method or an expansion in terms of spline functions. The accuracy and relative merits of these two methods is compared and contrasted. The influence of vertical eddy viscosity upon modal structure, and profiles of wind drift currents is examined for both homogeneous and stratified sea regions. The excitation and subsequent decay of the modes in response to a suddenly applied wind stress is considered, as is the influence of depth and viscosity upon the rate of convergence of expansions of vertical structure functions.

1. Introduction

Two dimensional storm surge models have been used extensively to study changes in sea surface elevation in response to various wind fields (e.g., Gjevik and Røed, 1976). In a two-dimensional model, bottom stress is related to the depth mean current. However physically bottom stress should be related to bottom current, and in deep water (e.g., areas off the Norwegian Coast, Gjevik and Røed, 1976; Røed, 1979) where the wind's momentum cannot penetrate to depth, bottom stress may be overestimated in a two dimensional model. Also vertically integrated models cannot compute the profile of wind induced currents; information which is important for pollution studies, particularly oil spills which depend upon a knowledge of surface currents (Weber, 1981). Current profiles are also of particular importance in determining the stresses on off-shore rigs (Gordon, 1982a, b). For these reasons, there is increasing interest in solving the three-dimensional equations which describe wind induced currents in a sea area. The solution of these equations can be computationally expensive, and consequently there is interest in methods which are computationally economic, and where possible can give some insight into the mechanisms controlling wind induced current profiles; the topic of this paper.

The solution of the three-dimensional hydrodynamic equations describing flow in both homogeneous (Koutitas, 1978; Davies and Owen, 1979; Cooper and Pearce, 1982) and stratified (Davies, 1981) sea regions has recently been developed using the Galerkin method in the vertical. In this approach the horizontal components of current are expanded in terms of coefficients varying with horizontal position and time, and functions (the basis functions) through the vertical. The choice of basis function is arbitrary, and a number of functions have been used, for example, cosine functions (Koutitas, 1978), a mixture of logarithmic and cosine functions (Cooper and Pearce, 1982), Chebyshev and Legendre polynomials (Davies and Owen, 1979; Gordon, 1982a). In general the application of the Galerkin method with an arbitrary basis set yields a set of coupled equations, which can be computationally expensive to integrate (Davies and Stephens, 1983).

An alternative to using the Galerkin method with an arbitrary set of basis functions is to choose the basis functions to be eigenfunctions of an eigenvalue problem describing the vertical variation of viscosity. These eigenfunctions are often termed vertical structure functions (Baker and Jordan, 1980, 1981) or simply modes (Heaps, 1972; Nihoul, 1977). Both terms will be used in this paper. In the case of a linear set of hydrodynamic equations, the use of modes in the vertical, yields a set of uncoupled equations which are computationally economic to integrate (Davies and Stephens, 1983).

In general, the determination of modes has been restricted to vertical variations of viscosity for which the eigenvalue problem can be solved analytically. The problem of constant eddy viscosity, and a slip bottom boundary condition was solved by Heaps (1972). Subsequently Heaps (1981), used a no-slip boundary condition and solved the eigenvalue problem in a two-layered approach in which within the bottom boundary layer, eddy viscosity increased linearly; with viscosity constant in the layer above it. An extension to a multilayer system, with viscosity linearly varying in each layer has recently been given by Furnes (1983). In the case in which viscosity varies in a parabolic manner, vertical structure functions (modes) have been computed in terms of expansions of Legendre and associated Legendre polynomials (Nihoul, 1977; Baker and Jordan, 1980, 1981). In this paper the linear modal equations describing three dimensional time dependent viscous flow are briefly developed using the Galerkin method, with an expansion of modes. By using the Runge-Kutta-Merson method or an expansion of spline functions, modes (vertical structure functions) can be accurately computed for arbitrary vertical variations of viscosity. The Runge-Kutta-Merson method of computing the modes is compared and contrasted with the alternative semi-analytical method of computing modes in terms of expansions of spline functions. The flexibility and accuracy of the methods are demonstrated by computing modes for a number of eddy viscosity profiles. The influence of vertical variations of eddy viscosity upon modal structure and hence current profiles is briefly illustrated in the later part of the paper.

2. Hydrodynamic equations

2.1. Development of the modal equations

In this section, the Galerkin method is used to develop the linear three dimensional modal equations in Cartesian Coordinates. Only the essential steps are given here and the interested reader is referred to Davies (1983a) for a more detailed development.

The linear hydrodynamic equations in sigma coordinates are given by (Davies, 1983a),

$$\frac{\partial \zeta}{\partial t} + \frac{\partial}{\partial x}\left(h \int_0^1 u \, d\sigma\right) + \frac{\partial}{\partial y}\left(h \int_0^1 v \, d\sigma\right) = 0 \tag{2.1}$$

$$\frac{\partial u}{\partial t} - \gamma v = -g \frac{\partial \zeta}{\partial x} + \frac{1}{h^2} \frac{\partial}{\partial \sigma}\left(\mu \frac{\partial u}{\partial \sigma}\right), \tag{2.2}$$

$$\frac{\partial v}{\partial t} + \gamma u = -g \frac{\partial \xi}{\partial y} + \frac{1}{h^2} \frac{\partial}{\partial \sigma}\left(\mu \frac{\partial v}{\partial \sigma}\right), \tag{2.3}$$

with $\sigma = z/h$. The advantages of using a sigma coordinate system and the development of the non-linear equations have been given in Davies (1980).

In the above equations, t denotes time, x, y, z, Cartesian coordinates forming a left handed set, and h depth of water, with ζ free surface elevation. Also u, v are components of current at depth z in the x, y directions respectively. The acceleration due to gravity g, and the geostrophic coefficient γ, are taken as constant, whereas the coefficient of vertical eddy viscosity μ in general depends upon x, y, z and t.

We now consider the development of the modal equations from (2.1). (2.2) and (2.3) using the Galerkin method in the vertical. Expanding the two components of velocity u, v in terms of m basis functions $f_r(\sigma)$ and coefficients $A_r(x, y, t)$ and $B_r(x, y, t)$ gives,

$$u = \sum_{r=1}^{m} A_r f_r(\sigma), \qquad v = \sum_{r=1}^{m} B_r f_r(\sigma). \tag{2.4}$$

Substituting (2.4) into (2.1) gives the modal form of the continuity equation, thus

$$\frac{\partial \zeta}{\partial t} + \sum_{r=1}^{m} \left(\frac{\partial}{\partial x}(A_r h) + \frac{\partial}{\partial y}(B_r h) \right) \int_0^1 f_r \, d\sigma = 0. \tag{2.5}$$

In general the choice of basis functions f_k and eddy viscosity μ which can be used with the Galerkin method is arbitrary (see Davies and Owen, 1980). Here we consider the case in which the vertical variation of μ is fixed, having a functional form denoted by $\psi(\sigma)$. Thus, expressing μ as,

$$\mu(x, y, \sigma, t) = \alpha(x, y, t)\, \psi(\sigma) \tag{2.6}$$

with $\alpha(x, y, t)$ representing the magnitude of μ which can vary with horizontal position and time.

For this variation of μ the basis functions $f_r(\sigma)$ can be determined as eigenfunctions of an eigenvalue problem of the form,

$$\frac{d}{d\sigma}\left[\psi \frac{df}{d\sigma}\right] = -\varepsilon f, \tag{2.7}$$

where ε are the associated eigenvalues.

Applying the Galerkin method to (2.2) (see Davies, 1983a, 1985 for details) and using the orthogonality property of eigenfunctions, namely

$$\int_0^1 f_r f_s \, d\sigma = 0 \qquad r \neq s, \qquad \neq 0 \qquad r = s, \tag{2.8}$$

then from (2.2), we obtain,

$$\begin{aligned} \frac{\partial A_k}{\partial t} \int_0^1 f_k f_k \, d\sigma = {} & \gamma B_k \int_0^1 f_k f_k \, d\sigma \\ & - g \frac{\partial \zeta}{\partial x} \int_0^1 f_k \, d\sigma - \frac{f_k(1)\, \tau_x^{\mathrm{h}}}{\rho h} \\ & + \frac{f_k(0) \tau_x^{\mathrm{s}}}{\rho h} - \frac{\alpha}{h^2} \sum_{i=1}^{m} A_i \psi \frac{df_i}{d\sigma} f_k \Big|_0^1 \\ & - A_k \frac{\alpha \varepsilon_k}{h^2} \int_0^1 f_k f_k d\sigma, \end{aligned} \tag{2.9}$$

where $k = 1, 2, \ldots, m$. In this equation and the corresponding equation derived from (2.3), τ_x^{s}, τ_y^{s}, and τ_x^{h}, τ_y^{h}, are the x and y components of surface stress denoted by superscript s, and bottom stress denoted by subscript h. Bottom stress can be computed from the bottom current u_{h}, v_{h} using either a quadratic law or a linear law of the form,

$$\tau_x^{\mathrm{h}} = k\rho u_{\mathrm{h}}, \qquad \tau_y^{\mathrm{h}} = k\rho v_{\mathrm{h}}, \tag{2.10}$$

with k a linear coefficient of bottom friction, and ρ density of sea water, here taken as constant.

An alternative to (2.10) is a no-slip condition, namely

$$u_{\mathrm{h}} = v_{\mathrm{h}} = 0. \tag{2.11}$$

Eqs. (2.9) are essentially an uncoupled set of modal equations, except for coupling through bottom friction and the term

$$\sum_{i=1}^{m} A_i \psi \frac{df_i}{d\sigma} f_k \Big|_0^1 .$$

We now consider how this coupling can be removed by an appropriate choice of surface and sea bed boundary conditions for the modes f_r.

In order to determine a unique set of eigenfunctions from (2.7) it is necessary to specify sea surface and sea bed conditions for the eigenfunctions f_r. In the case of the no slip bottom boundary condition, eq. (2.11), then $f_r(1) = 0$ for all r.

Considering the surface boundary condition; the eigenfunctions and eigenvalues of (2.7) will be real (Davies, 1983a), provided

$$\frac{df_r}{d\sigma}\Big|_0 = C_1 f_r(0), \tag{2.12a}$$

with C_1 an arbitrary constant.

Similarly when a slip condition is applied at the sea bed, we have,

$$\frac{df_r}{d\sigma}\Big|_1 = C_2 f_r(1), \tag{2.12b}$$

with C_2 an arbitrary constant.

Davies (1983b) showed that by choosing these coefficients in an appropriate manner, the rate of convergence of expansions (2.4) could be enhanced.

An alternative to (2.12b) when a linear slip bottom boundary condition is applied is to satisfy this boundary condition exactly. Thus, applying a linear slip condition at the sea bed, using (2.10), gives

$$\tau_x^h = \frac{-\mu}{h}\frac{\partial u}{\partial \sigma}\bigg|_1 = k u_h$$
$$\tau_y^h = \frac{-\mu}{h}\frac{\partial v}{\partial \sigma}\bigg|_1 = k v_h, \qquad (2.13a)$$

When expansions (2.4) are substituted into (2.13a), the bottom boundary condition becomes,

$$\frac{\mathrm{d}f_r}{\mathrm{d}\sigma}\bigg|_1 = \frac{-kh}{\mu(1)} f_r\bigg|_1. \qquad (2.13b)$$

A boundary condition of the form (2.13b) has been used previously (Heaps, 1972). However, in a sea region in which the depth h varies, the term $kh/\mu(1)$ has to be constant, in order to ensure that the same basis functions are employed at each horizontal grid point. By treating the bottom boundary condition as a natural boundary condition (Davies, 1983a) and using (2.12b) this problem can be overcome (see Davies, 1983a for details).

Conditions (2.12a) and (2.12b) and (2.13b) together with the normalization condition, taken for convenience as

$$f_r(0) = 1 \qquad \text{for all } r, \qquad (2.14)$$

are sufficient to determine a unique solution of (2.7) in the case of a slip bottom boundary condition. (In the case of a no-slip boundary condition, eqs. (2.11), and (2.14) are applied, with $f_r(1) = 0$ for all r.)

For the particular case in which $C_1 = C_1 = 0$, then from (2.9) we have,

$$\frac{\partial A_k}{\partial t} = \gamma B_k - g\frac{\partial \zeta}{\partial x} a_k \Phi_k - \frac{f_k(1)}{\rho h}\tau_x^h \Phi_k + \frac{\tau_x^s}{\rho h}\Phi_k - \frac{\alpha}{h^2} A_k \varepsilon_k, \qquad (2.15)$$

and from the v equation of motion, we have

$$\frac{\partial B_k}{\partial t} = -\gamma A_k - g\frac{\partial \zeta}{\partial y} a_k \Phi_k - \frac{f_k(1)}{\rho h}\tau_y^h \Phi_k + \frac{\tau_y^s}{\rho h}\Phi_k - \frac{\alpha}{h^2} B_k \varepsilon_k, \qquad (2.16)$$

with

$$\Phi_k = 1\bigg/\int_0^1 f_k^2\,\mathrm{d}\sigma, \qquad a_k = \int_0^1 f_k\,\mathrm{d}\sigma. \qquad (2.17)$$

2.2. *Calculation of vertical modes*

In the case in which ψ is constant, or varies in a parabolic manner, the eigenfunctions [modes or vertical structure functions (Baker and Jordan (1980)] of (2.7) can be determined analytically (Heaps, 1972; Baker and Jordan, 1980, 1981). However for many physically realistic variations (Smith, 1982; Wolf, 1980), an analytic solution is not possible.

In this section we consider two methods whereby the eigenvalues and eigenfunctions of (2.7) can be computed, and the necessary integrals Φ_k and a_k (eq. 2.17) required in the spectral model can be determined. By using two methods it is possible to check the accuracy of each, and to determine under what conditions numerical difficulties may occur.

2.2.1. Application of the Galerkin method. In the first method, eq. (2.7) is solved using the Galerkin method (Davies, 1983a, b). In this method the eigenfunction f_r is expanded in terms of a set of $\bar{m}$ coefficients d_{ir} and B-spline M_i, giving

$$f_r = \sum_{i=1}^{\bar{m}} d_{ir} M_i(\sigma). \qquad (2.18)$$

The piecewise nature of the B-splines enables essential boundary conditions to be incorporated by linearly combining the splines. Their piecewise nature also means that resolution can be improved in high shear layers (see Davies, 1983a), where the eigenfunctions change most rapidly through the vertical, by increasing the number of knots, and reducing their spacing (see Davies, 1983a for details).

Applying the Galerkin method to (2.7), the rth eigenequation is multiplied by f_k and integrated over the region 0 to 1. When the term involving ψ is integrated by parts, we obtain,

$$\psi\frac{\mathrm{d}f_r}{\mathrm{d}\sigma}f_k\bigg|_1 - \psi\frac{\mathrm{d}f_r}{\mathrm{d}\sigma}f_k\bigg|_0 - \int_0^1 \psi\frac{\mathrm{d}f_r}{\mathrm{d}\sigma}\frac{\mathrm{d}f_k}{\mathrm{d}\sigma}\,\mathrm{d}\sigma = -\varepsilon_r\int_0^1 f_r f_k\,\mathrm{d}\sigma \qquad (2.19)$$

where $k = 1, 2, \ldots, m$. The first two terms in (2.19) involve vertical derivatives of the basis functions at sea surface and sea bed. By eliminating these terms using for example (2.12), a unique solution of (2.7) can be determined, with computed eigenfunctions satisfying those conditions.

When (2.18) is substituted into (2.19) a standard eigenvalue problem is obtained which can be readily solved to determine the coefficients d_{ir} and eigenvalues ε_r. Details can be found in Davies (1983a) and will not be repeated here.

2.2.2. Solution using the Runge-Kutta-Merson method. An alternative to using the Galerkin method with an expansion of B-splines, is to solve the eigenvalue problem (2.7) using an iterative method to determine the eigenvalue ε_i. In the iterative method, the Runge-Kutta-Merson technique is employed to integrate the eigen-equation from sea surface to sea bed, and to compute the integrals $a_i = \int_0^1 f_i \, d\sigma$ and $\Phi_i = 1/\int_0^1 f_i^2 \, d\sigma$ used in eqs. (2.5), (2.15) and (2.16).

The Runge-Kutta-Merson technique is a method of integrating a system of coupled differential equations of the form,

$$\frac{dY_i}{d\sigma} = F_i(\sigma, Y_1, Y_2, \ldots, Y_n) \quad \text{where } i = 1, 2, \ldots, n. \tag{2.20a}$$

In this coupled set of differential equations, Y_i is the variable to be integrated (in our case) over the region $0 \leqslant \sigma \leqslant 1$. In general Y_i is an arbitrary function F_i of σ and the variables Y_1, $Y_2, \ldots Y_n$.

Considering for illustrative purposes the single differential equation

$$\frac{dY}{d\sigma} = F(\sigma, Y). \tag{2.20b}$$

Starting from $Y(\sigma_0)$, then the fourth order Runge-Kutta-Merson method generates a solution $Y(\sigma_0 + \Delta\sigma)$ at a step size $\Delta\sigma$ from σ_0, using

$$Y(\sigma_0 + \Delta\sigma) = Y(\sigma_0) + \tfrac{1}{6}(\Delta_1 + 2\Delta_2 + 2\Delta_3 + \Delta_4), \tag{2.20c}$$

where

$$\begin{aligned}
\Delta_1 &= \Delta\sigma\, F[\sigma_0, Y(\sigma_0)] \\
\Delta_2 &= \Delta\sigma\, F[\sigma_0 + \tfrac{1}{2}\Delta\sigma, Y(\sigma_0) + \tfrac{1}{2}\Delta_1] \\
\Delta_3 &= \Delta\sigma\, F[\sigma_0 + \tfrac{1}{2}\Delta\sigma, Y(\sigma_0) + \tfrac{1}{2}\Delta_2] \\
\Delta_4 &= \Delta\sigma\, F[\sigma_0 + \Delta\sigma, Y(\sigma_0) + \Delta_3].
\end{aligned}$$

The method therefore requires four function evaluations per integration step, which makes it very time consuming, particularly with a small integration step $\Delta\sigma$. The particular problem considered here of solving (2.7) and determining the integrals a_i and Φ_i, can be expressed as four differential equations, of the form,

$$\frac{dY_1}{d\sigma} = Y_2/\psi, \qquad \frac{dY_2}{d\sigma} = -\varepsilon_r Y_1,$$
$$\frac{dY_3}{d\sigma} = Y_1, \frac{dY_4}{d\sigma} = Y_1^2, \tag{2.21}$$

where

$$Y_1 = f_r, \qquad Y_2 = \psi df_r/d\sigma,$$
$$Y_3 = \int_0^\sigma f_r \, d\sigma, \; Y_4 = \int_0^\sigma f_r^2 \, d\sigma;$$

consequently, $a_i = Y_3$, and $\Phi_i^{-1} = Y_4$.

In this paper, a fourth order Runge-Kutta-Merson method is used to integrate (2.21) through the vertical. This method estimates the error in the solution at each step $\Delta\sigma$ in the vertical (Hall and Watt, 1976; Hamming, 1962). If this error is greater than a prescribed criterion, the vertical step size $\Delta\sigma$ is reduced. By this means an accurate solution can be obtained even in regions where the mode changes very rapidly. The advantage of this is discussed in the next section.

Considering now the method of determining the eigenvalues ε_r and eigenfunctions f_r, together with integrals a_r and Φ_r.

For large r, the positive eigenvalues of (2.7) can be estimated from (see Appendix),

$$\tilde{\varepsilon}_r = \left[r\pi / \int_0^1 (1.0/\sqrt{\psi}) \, d\sigma \right]^2,$$

where $\tilde{\varepsilon}_r$ denotes an estimated eigenvalue.

Hence the first r positive eigenvalues of (2.7) lie in the interval between zero and $\tilde{\varepsilon}_r + E$, where E is a small fraction of $\tilde{\varepsilon}_r$ which is added to ensure that ε_r lies within this interval.

The calculation then proceeds in the following steps:

(1) By making an initial estimate (denoted by superscript) of the first eigenvalue $\varepsilon_1^{(1)}$ which is usually taken as zero.

(2) The Runge-Kutta-Merson method as described above is used to integrate (2.7) in order to compute the value of $df_1^{(1)}/d\sigma$ and $f_1^{(1)}$

at the sea bed, for specified surface values of $\mathrm{d}f_1^{(1)}/\mathrm{d}\sigma$ and f_1 determined by eqs. (2.12a) and (2.14).

(3) For the case of a slip bottom boundary condition given by (2.12b), the difference between the value of $\mathrm{d}f_1^1/\mathrm{d}\sigma$ at the sea bed and that specified in (2.12b) is determined. For the boundary condition given by (2.13a), the difference between $\mathrm{d}f_1^1/\mathrm{d}\sigma$ and $-[(kh/\mu(1)]f_1^{(1)}$ at the sea bed is determined. With a no slip condition (eq. 2.11), the difference between $f_1^{(1)}$ and zero is computed.

(4) A revised estimate of the first eigenvalue $\varepsilon_1^{(2)}$ is determined by increasing $\varepsilon_1^{(1)}$ by a small step size δ i.e. $\varepsilon_1^{(2)} = \varepsilon_1^{(1)} + \delta$. Steps two and three are then repeated until two eigenvalues $\varepsilon_1^{(m-1)}$ and $\varepsilon_1^{(m)}$ have been determined such that in the case of the slip boundary, the values of $\mathrm{d}f_1^{(m-1)}/\mathrm{d}\sigma$ and $\mathrm{d}f_1^{(m)}/\mathrm{d}\sigma$ bracket the exact sea bed condition. In the case of the no slip condition, values of $f_1^{(m-1)}$ and $f_1^{(m)}$ bracketing zero are determined.

(5) Having bracketed the value of ε_1 by this means, the accuracy of the eigenvalue can then be improved by using Newtons method to ensure that the sea bed boundary condition is satisfied to within a given degree of precision. The interested reader is referred to text books on numerical analysis (e.g. Hamming, 1962) for details of Newtons method.

(6) The Runge-Kutta-Merson method is then used to determine the integrals a_1 and Φ_1, required in the spectral model, together with mode f_1.

Once the first eigenvalue and eigenfunction have been determined, then an estimate of the second eigenvalue is computed by incrementing ε_1 by δ and the above procedure is repeated until the first r eigenvalues have been found. To ensure that no eigenvalues and associated eigenfunctions are omitted in this stepping method it is necessary to choose δ to be a small fraction of the interval from zero to $\tilde{\varepsilon}_r + E$. A simple check that ensures that an eigenfunction is not omitted is to compute the number of times it goes to zero in the vertical, which must increase by one, as the mode number increases (see Fig. 2).

Vertical modes, eigenvalues ε_r, and integrals a_r and Φ_r computed using either the Runge-Kutta-Merson method, or the expansion in terms of splines may then be used in eqs. (2.5), (2.15), and (2.16).

3. Computation of vertical modes [vertical structure functions] and steady state profiles

3.1. A homogeneous sea region

In a preliminary series of calculations both the Runge-Kutta-Merson method and the expansion in terms of splines, were used to compute vertical modes in order to compare the methods and test their accuracy.

Initially the distribution of eddy viscosity shown in Fig. 1, profile (a) was employed with μ constant at 1000 cm^2 s^{-1} from sea surface to sea bed, and a no-slip condition at the sea bed. In this case an analytical solution can be found (Davies, 1983a) with which numerical solutions can be compared.

Values of $\alpha\varepsilon_r$, Φ_r and a_r computed with the Runge-Kutta-Merson method were in excellent agreement (to better than 6 figures in the first 6

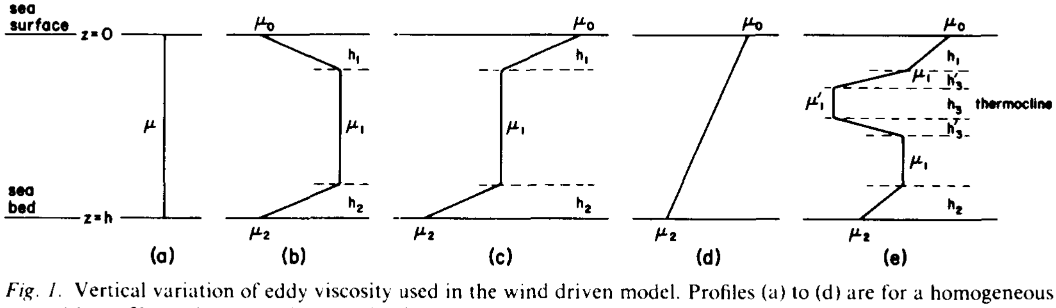

Fig. 1. Vertical variation of eddy viscosity used in the wind driven model. Profiles (a) to (d) are for a homogeneous sea, with profile (e) incorporating a reduction in turbulence at the level of the thermocline, reflecting enhanced vertical stability in the region.

modes) with the analytical solution. Excellent agreement was also obtained with the spline method, using the order of 25 equally spaced splines in the vertical.

Although a constant value of eddy viscosity is appropriate for an initial examination of the accuracy of the methods, since an analytical solution is available, it is not physically appropriate. Eddy viscosity values found from current measurements (Bowden et al., 1959; Bowden, 1978; Wolf, 1980) and from turbulence theory (Smith, 1982) have suggested that a constant value of eddy viscosity is not physically realistic for wind driven currents in a tidal sea.

Neumann and Pierson (1964) give an empirical formula for surface eddy viscosity μ_0 of the form,

$$\rho\mu_0\,(\mathrm{cm}^{-1}\,\mathrm{gr}\,\mathrm{s}^{-1}) = 0.1825 \times 10^{-4}\, W^{5/2}\,(W \text{ in cm/s}). \qquad (3.1)$$

By using Reynolds stress relationships due to Ichiye (1967) to relate surface eddy viscosity to the wave field, and equations (Carter, 1982) to determine the wave field in terms of wind velocity, W. Davies (1984a, b) derived the following equation for surface eddy viscosity, in a fully developed wave field.

$$\mu_0\,(\mathrm{m}^2\,\mathrm{s}^{-1}) = 0.3043 \times 10^{-4}\, W^3\,(W \text{ in m/s}). \qquad (3.2)$$

Values of eddy viscosity for a range of wind speed computed with (3.1) and (3.2) are shown in Table 1.

At depth, eddy viscosity can be related to the current velocity using (Davies and Furnes, 1980).

$$\mu_1 = k(u^2 + v^2)/\sigma, \qquad (3.3)$$

where $\sigma = 10^{-4}\,\mathrm{s}^{-1}$, $k = 2.0 \times 10^{-5}$. In the central Northern North Sea (depth h taken as 100 m) tidal and strong wind driven currents are typically of the order of 75 cm/s, giving from (3.3)

Table 1. *Values of surface eddy viscosity μ_0 for a range of wind speeds, computed using (A) an equation taking into account the wave field and (B) an empirical equation of Neumann and Pierson (1964)*

W (m/s)	5	10	15	20	25
μ_0 (cm^2/s) A	40	316	1069	2535	4951
μ_0 (cm^2/s) B	100	563	1551	3184	5563

a μ_1 value of order 1000 cm^2/s during major wind events.

At the sea bed, eddy viscosity depends upon the roughness length z_0 and current velocity (Bowden et al., 1959; Bowden, 1978). From observations, Channon and Hamilton (1971) found a range of z_0 values, typically from 7.0 cm to 0.44 cm. Using this range of z_0 values, with strong tidal and wind driven currents in the North Sea, Davies (1983a), suggested that eddy viscosity at the sea bed could vary from 100 cm^2/s to below 1 cm^2/s depending upon current velocity and z_0 value. In the calculations described later, $\mu_2 = 50$ cm^2/s; a value lying midway in this range.

We shall now consider the influence upon the accuracy of the spline and Runge-Kutta-Merson methods of using a vertically varying eddy viscosity profile covering the range of viscosity described above.

Fig. 1, profile (b) shows a typical vertical variation of eddy viscosity which is probably appropriate in a strong tidal current regime (velocity of order 75 cm/s), at low wind speed ($W \approx 5$ m/s). From Table 1, it is evident that at $W = 5$ m/s, μ_0 is of order 50 cm^2/s, and for currents at depth of order 75 cm/s, $\mu_1 = 1000$ cm^2/s (eq. 3.3), with $\mu_2 = 50$ cm^2/s. Bowden et al. (1959) suggests that the distance h_2 over which μ increases linearly from its sea bed value should be of order 0.1 h. Here we take for illustrative purposes $h_1 = h_2 = 0.1\ h = 10$ m. [The value of h_1 should be related to the frictional velocity u_* at the sea surface and hence to the surface stress (Davies, 1985). A value of order 10 m however is appropriate (Davies, 1985).]

Values of $\alpha\varepsilon_r$, Φ_r and a_r, computed using the viscosity profile given in Fig. 1(b) with $\mu_0 = 50$ cm^2/s, $\mu_1 = 1000$ cm^2/s, $\mu_2 = 50$ cm^2/s, are given in Table 2 (column 1). With this profile of viscosity, significant errors occurred with an equally spaced distribution of splines. However an accurate solution was obtained with the Runge-Kutta-Merson method or when an expansion of the order of forty splines, distributed so that there was an increased number of splines in the near surface and near bed regions was employed.

To understand why there is a significant error in the eigenvalues and eigenfunctions computed with a small number of splines, when $\mu_0 = \mu_2 = 50$ cm^2/s, $\mu_1 = 1000$ cm^2/s but not

Table 2. *Values of $\alpha\varepsilon_r$, Φ_r and a_r computed using the viscosity profiles shown in Fig. 1(b), 1(c), 1(d) and 1(e), with a range of μ_0, μ_1, μ_2 values. Both slip and no-slip bottom boundary conditions were used*

No slip bottom boundary condition			Slip bottom boundary condition			Stratified	
$\mu_0 = 50$ cm^2/s $\mu_1 = 1000$ cm^2/s $\mu_2 = 50$ cm^2/s (Fig. 1(b))	$\mu_0 = 5000$ cm^2/s $\mu_1 = 1000$ cm^2/s $\mu_2 = 50$ cm^2/s (Fig. 1(c))	$\mu_0 = 5000$ cm^2/s $\mu_2 = 50$ cm^2/s (Fig. 1(d))	$\mu_0 = 50$ cm^2/s $\mu_1 = 1000$ cm^2/s $\mu_2 = 50$ cm^2/s (Fig. 1(b))	$\mu_0 = 5000$ cm^2/s $\mu_1 = 1000$ cm^2/s $\mu_2 = 50$ cm^2/s (Fig. 1(c))	$\mu_0 = 5000$ cm^2/s $\mu_2 = 50$ cm^2/s (Fig. 1(d))	$\mu_1' = 500$ cm^2/s (Fig. 1(e))	$\mu_1' = 50$ cm^2/s (Fig. 1(e))
0.169	0.169	0.149	0.0	0.0	0.0	0.166	0.126
1.629	1.643	3.037	0.981	0.987	1.903	1.430	0.456
4.819	4.946	8.965	3.855	3.939	6.583	4.040	2.564
9.767	10.295	17.898	8.414	8.799	14.154	8.993	4.652
16.274	17.719	29.826	14.350	15.423	24.663	16.142	8.703
24.157	27.125	44.745	21.438	23.694	38.137	24.333	14.824
1.697	1.663	1.276	1.0	1.0	1.0	1.774	3.494
2.050	1.696	1.125	2.138	1.907	1.042	2.271	1.947
2.698	1.580	1.111	2.585	1.674	1.066	1.494	0.325
3.753	1.368	1.107	3.403	1.396	1.078	0.835	0.764
5.151	1.152	1.105	4.545	1.146	1.085	0.837	0.110
6.273	0.972	1.103	5.656	0.965	1.089	0.912	0.384
0.732	0.739	0.867	1.000	1.000	1.000	0.713	0.455
−0.173	−0.190	−0.140	0.0	0.0	0.0	−0.166	−0.333
0.069	0.091	0.078	0.0	0.0	0.0	0.105	0.324
−0.035	−0.058	−0.054	0.0	0.0	0.0	−0.084	−0.082
0.022	0.046	0.042	0.0	0.0	0.0	0.056	0.242
−0.016	−0.041	−0.034	0.0	0.0	0.0	−0.042	−0.061

when μ is constant at 1000 cm^2/s, it is necessary to examine the vertical variation of the first few eigenfunctions (Fig. 2). It is apparent from Fig. 2, profiles (a) and (b) that when μ is reduced in the sea surface and sea bed regions, compared with its mean value, then there is a significantly larger shear in these regions, than when μ is constant at its mid-depth value. In order to accurately resolve the high shear which occurs when μ_0 and μ_2 are low (of order 50 cm^2/s), it is necessary to increase the number of splines in the high shear regions. However when μ is constant these high shear regions are absent (see Fig. 2, profile (a)) and modal structure can be accurately computed with a lower number of splines.

The Runge-Kutta-Merson method however remained accurate in both cases. This is because this technique uses a multiple stepping method with a variable step size in performing the integration. At each step an estimate of the error is made and if this is found to be above a certain prescribed limit the step size is reduced. (Details of the method can be found in numerical analysis text books, e.g. Hall and Watt, 1976.) Consequently the step size is reduced in regions where the eigenfunction changes most rapidly and accuracy is preserved. Calculations showed that the Runge-Kutta-Merson method required more computer time than the Spline approach. However in practice when a modal method is used to solve the hydrodynamic equations, the calculation of the modes is a very small fraction of the computer time, the majority of which is spent in integrating the modal equations through time.

At high wind speeds ($W = 25$ m/s), μ_0 is of order 5000 cm^2/s, and the profiles (c) or (d) shown in Fig. 1 may then be applicable. Values of $\alpha\varepsilon_r$, Φ_r and a_r, computed using eddy viscosity profiles (b), (c) and (d), with both slip and no-slip bottom boundary conditions are given in Table 2. Both the Spline method and the Runge-Kutta-Merson method gave identical values of ε_r, Φ_r and a_r.

Referring to Table 2, it is evident that the eigenvalue increases with mode number, and that for a given mode the eigenvalues are comparable in magnitude. It is interesting to note that in the case of the slip bottom boundary condition, $\varepsilon_1 = 0$, and consequently the first mode is only damped by bottom friction.

Considering the weighting functions Φ_r. It is apparent from Table 2 that for viscosity profiles (c) and (d), Φ_r values for all the modes are comparable in magnitude. However in the case of distribution (b), the Φ_r values of the higher modes exceed those of the lower modes. The importance of this is discussed below.

It is evident from eqs. (2.15) and (2.16), that the initial response of a sea region to a suddenly applied wind stress is the excitation of all vertical modes. The contribution of these modes to the initial current profile is determined by the weighting term Φ_r. Consequently in the case of viscosity profile (b) for which the Φ_r values of some of the higher modes, exceed those of the lower modes, these higher modes will contribute most to the current's profile following the sudden imposition of a wind stress. However as time progresses the coefficients of the modes are damped by the term $\alpha\varepsilon_r/h^2$. Since ε_r increases with mode number, the higher modes are damped most rapidly and hence as time progresses these modes contribute less to the current profile. In the case of a wind impulse, in shallow water ($h \leqslant 100$ m), then the contribution of the higher modes decreases very rapidly and an accurate profile can be computed using the order of ten modes. In deep water ($h \approx 1000$ m), because of the h^{-2} dependence of the damping then the higher modes persists much longer and a significantly larger number of modes are required (of order 30), to compute an accurate profile. As μ_0 is reduced, the Φ_r terms for the higher modes increase, and hence their contribution to the current profile is increased. Consequently a larger number of modes are required to compute an accurate current profile when μ_0 is low (of order 50 cm^2/s), than when μ_0 is high (of order 5000 cm^2/s) relative to its mean value. The depth mean value of viscosity is also important in determining the rate of damping of the modes, and it is evident from eqs. (2.15) and (2.16) that damping increases with increasing α. It is important to note that α takes into account the time variation of viscosity, and hence (2.15) and (2.16) can be readily solved with a spatial and temporally varying viscosity.

Since modal damping is determined by the term $\alpha\varepsilon_r/h^2$, then current profiles will reach a steady state more rapidly when the depth mean eddy viscosity is high, and water depth shallow,

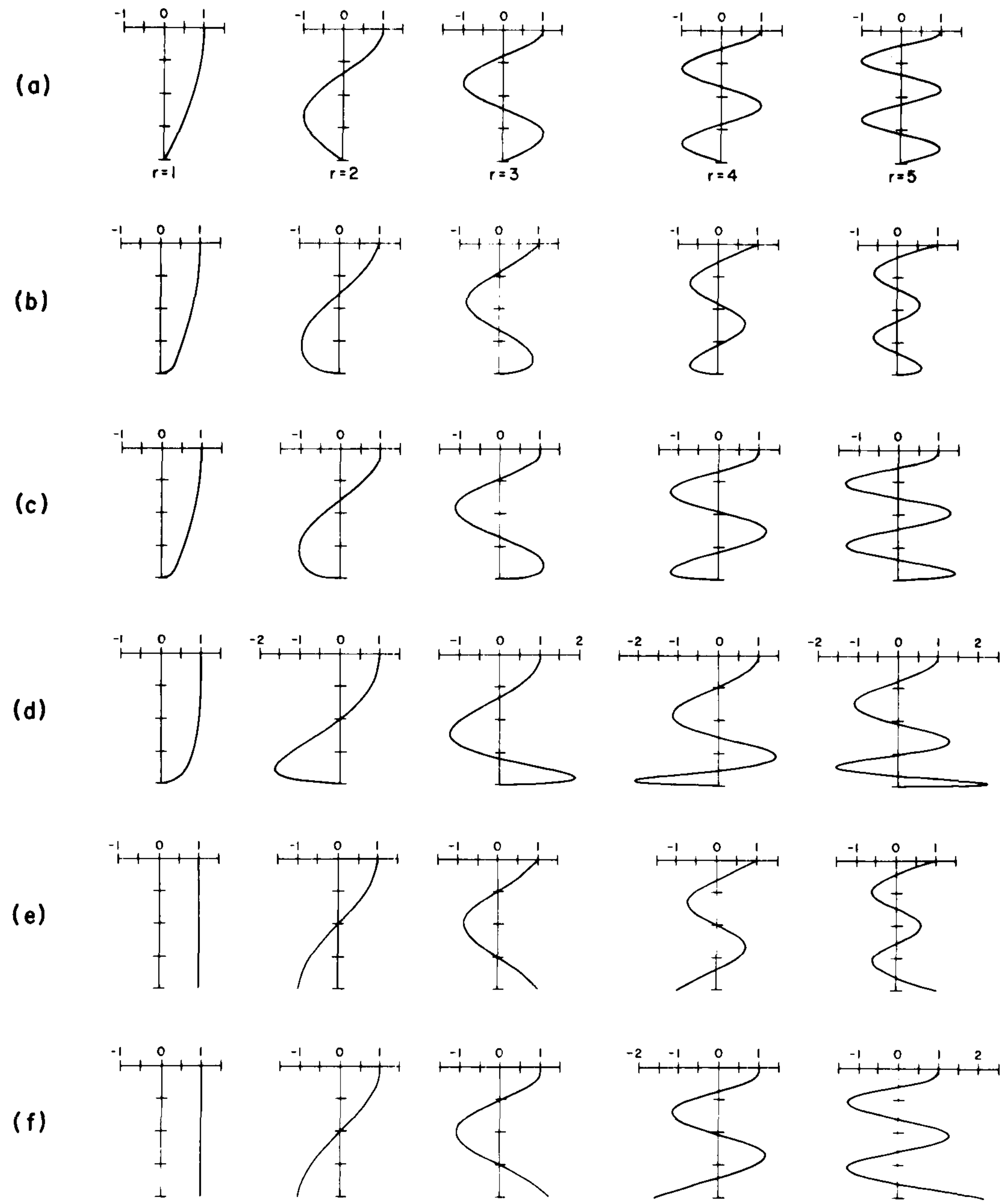

Fig. 2. Vertical variation of the first five modes in a water depth $h = 100$ m, with $h_1 = h_2 = 10$ m, computed with: (a) Profile in Fig. 1(a), using a no slip condition with μ constant at 1000 cm²/s; (b) profile in Fig. 1(b), using a no slip condition with $\mu_0 = 50$, $\mu_1 = 1000$, $\mu_2 = 50$ cm²/s; (c) profile in Fig. 1(c), using a no slip condition with $\mu_0 = 5000$, $\mu_1 = 1000$, $\mu_2 = 50$ cm²/s; (d) profile in Fig. 1(d), using a no slip condition with $\mu_0 = 5000$, $\mu_2 = 50$ cm²/s; (e) profile in Fig. 1(b), using a slip condition with $\mu_0 = 50$, $\mu_1 = 1000$, $\mu_2 = 50$ cm²/s; (f) profile in Fig. 1(c), using a slip condition with $\mu_0 = 5000$, $\mu_1 = 1000$, $\mu_2 = 50$ cm²/s.

than in a low viscosity deep water region. A conclusion born out by calculations (Davies, 1985, 1986).

In the case of a slip bottom boundary condition, the rate of damping of the modes is complicated by the presence of bottom stress, the magnitude of which depends upon bottom current, which contains a contribution from all modes (see eq. 2.10). The influence of bottom friction on the modal structure of current profiles is considered in Davies (1984b). It should be noted that in the case of a slip bottom, with modes computed using boundary conditions (2.12b), with $C_2 = 0$, then the eigenvalue of the first mode is zero (Table 2), and damping of this mode is produced only by bottom friction.

Considering the magnitude of the terms a_r, which determine the distribution between the modes of the forcing due to gradients of sea surface elevation (eqs. (2.15) and (2.16)). In the case of the slip bottom boundary condition, only a_1 is non zero and hence gradients of sea surface elevation can only directly contribute to changes in coefficients A_1, B_1. In the case of the no-slip bottom boundary condition, for the cases considered in Table 2; a_1 is dominant, and the a_r alternate in sign. Changes with time in gradients of sea surface elevation therefore affect the time variation of all the modes, with a weighting determined by the terms $a_r \Phi_r$, $b_r \Phi_r$.

Comparing vertical structure functions (modes) in Fig. 2, computed with the no-slip bottom boundary condition for a range of viscosity profiles (see caption). It is evident that for a given viscosity profile, as the mode number increases, the oscillatory nature of the functions increases; a requirement of orthogonal functions. Also near surface and near bed shear increases with mode number. It is evident that as μ_0 is reduced from 5000 cm^2/s to 50 cm^2/s then near surface shear particularly in the higher modes is increased.

Modes computed using a slip bottom boundary condition [see Fig. 2, profiles (e) and (f)] show a similar vertical variation to those computed using a no-slip condition. However in this case the first mode is constant, and is independent of viscosity profile. Also it is the only mode which contributes to the net transport of fluid. Since only $a_1 = \int_0^1 f_1 \, d\sigma$ is non zero, then from the continuity equation (2.5) only this mode can contribute to changes in sea surface elevation.

Steady state wind drift currents, computed with both slip and no-slip bottom boundary conditions for various eddy viscosity distributions are shown in Fig. 3 (profiles (a), (b)). (See caption to figure for eddy viscosity values.) For illustrative purposes, a wind stress of $\tau_x = 0.0$, $\tau_y = -10$ dP_a corresponding to a northerly wind (the dominant wind over the North Sea) was used in these calculations. Since the model is linear, the profiles shown in Fig. 3, can be scaled to any wind stress. In the case of the slip bottom boundary condition, a value of $k = 0.002$ m/s was used, an appropriate value for the North Sea (Heaps, 1972).

It is evident from Fig. 3, that as μ_0 is reduced from 5000 cm^2/s to 50 cm^2/s then near surface shear is increased, in the v-component of current (the component in the wind direction). This is to be expected, and reflects the change in near surface shear found in the vertical structure functions (modes), (see Fig. 2). No significant near

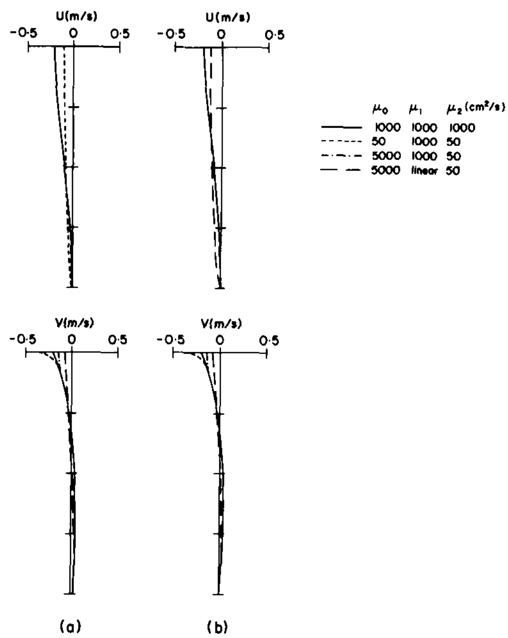

Fig. 3. Steady state u and v components of drift current computed with a wind stress $\tau_x = 0.0$, $\tau_y = -10$ dP_a for a range of eddy viscosities (cm^2/s) as shown in key. Computed: (a) with a slip condition $k = 0.002$ m/s; (b) with a no-slip condition.

surface shear occurs in the u component of current (the component at right angles to the wind field), which shows a near linear variation with depth.

It is apparent from Fig. 3(a), (b) that near the sea surface current profiles computed with the slip and no-slip bottom boundary conditions are not significantly different. This is to be expected, since in a depth of 100 m, little of the wind's energy can penetrate to the sea bed and hence the bottom boundary condition has little effect. Although the vertical modes, computed with slip and no-slip are significantly different in the sea bed region (see Fig. 2), the coefficients computed with the spectral model, are such that expansions (2.4) give current profiles which are not significantly different near the sea bed, reflecting the physical nature of the solution.

3.2. *A stratified sea region*

In a stratified sea, a reduction in eddy viscosity within the thermocline (or pycnocline) due to enhanced vertical stability (Mortimer, 1952; Mork, 1972) will occur and this has to be taken into account in the assumed vertical variation of viscosity.

A vertical profile of viscosity reflecting a wind-induced turbulent surface layer of thickness h_1, with viscosity reducing linearly from μ_0 to μ_1 is shown in Fig. 1(e). Below this surface layer eddy viscosity decreases over a region h'_3 to a low value μ'_1 applying within the thermocline. At depth, in the region below the thermocline viscosity increases over a region h'_3, to its value μ_1. A region of decreasing turbulence over a distance h_2 near the sea bed, to a value μ_2 is shown in Fig. 1(e).

In the calculations described here, μ_0 was set at 5000 cm^2/s, with μ_1 at 1000 cm^2/s and μ_2 at 50 cm^2/s. The thickness of the bottom layer was set at $h_2 = 10$ m; within the thermocline, $h'_3 = 2$ m and $h_3 = 6$ m, giving a total thermocline thickness of 10 m, typical of the central North Sea (Davies, 1981). In order to examine the effect of changes in mixed layer thickness h_1, and viscosity μ'_1 within the thermocline upon modal structure, calculations were performed with $h_1 = 10$ m (a shallow thermocline) and $h_1 = 40$ m (a deeper thermocline), with $\mu'_1 = 50$ cm^2/s (a strong thermocline) and $\mu'_1 = 500$ cm^2/s (a weak thermocline).

Values of $\alpha\varepsilon_r$, Φ_r and a_r computed with $h_1 = 10$ m; $\mu'_1 = 500$ cm^2/s and 50 cm^2/s using viscosity profile 1(e), characterizing stratified conditions, are given in Table 2. In order to be able to accurately compute modal structure when $\mu'_1 = 50$ cm^2/s an enhanced distribution of splines, was required in the region of the thermocline. The reason for this can be appreciated from Fig. 4. It is apparent from Fig. 4 (profile (a)) that with $\mu'_1 = 500$ cm^2/s, the modes show no significant vertical shear at the level of the thermocline. However when μ'_1 is reduced to 50 cm^2/s, a high shear region is evident at the level of the thermocline, and the higher modes exhibit larger oscillations below the thermocline (compare Fig. 4, profiles (a) and (b)). This difference in vertical structure, particularly in the higher modes, explains why spline resolution in the region of the thermocline must increase as μ'_1 is reduced.

Also shown in Fig. 4 (profile (c)) are vertical structure functions computed with identical values of μ to those used in profile (b), but with $h_1 = 40$ m. Comparing Fig. 4 ((b) and (c)) it is evident that in both cases a region of rapid shear occurs within the thermocline, although when $h_1 = 40$ m, this occurs at approximately mid-depth, rather than near the surface ($h_1 = 10$ m). In the case of $h_1 = 40$ m, in the higher modes ($r = 3, 4$ or 5), the magnitude of the mode decreases significantly from its surface value, and changes sign above the thermocline. In the case of $h_1 = 10$ m, the mode remains essentially constant above the thermocline. This point will be discussed further in connection with the steady state profiles described later.

Modes computed using the slip bottom boundary condition are also shown in Fig. 4 (profile (d)). The nature of these modes is such that the first mode is constant. The higher modes show a similar vertical structure to those computed with profile (c), except in the region near the sea bed, where modes computed with the slip condition are not constrained to be zero at the bed. It is evident from a comparison of modes $r = 4$ and $r = 5$, computed with profiles (c) and (d), that their vertical variation in the near surface and thermocline region are not significantly different.

Steady state profiles of wind drift currents computed with $h_1 = 10$ m and $\mu'_1 = 500$ cm^2/s and 50 cm^2/s are given in Fig. 5, profiles (a) and (b). For consistency with the previous calculations, a wind stress $\tau_x = 0.0$, $\tau_y = -10$ dP_a was used in these computations. Comparing these profiles it is

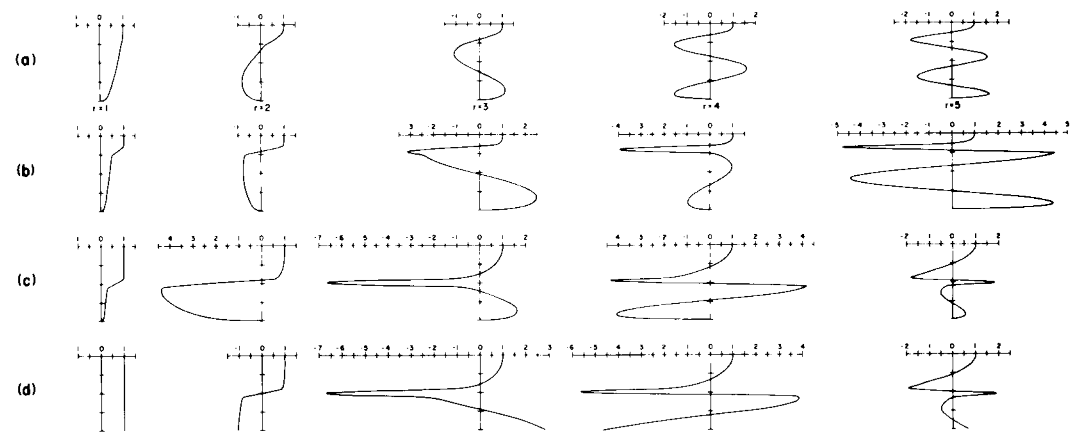

Fig. 4. Vertical variation of the first five modes in a water depth $h = 100$ m, computed using the viscosity profile shown in Fig. 1(e), with $h'_3 = 2$ m, $h_3 = 6$ m, $h_2 = 10$ m, $\mu_0 = 5000$ cm²/s, $\mu_1 = 1000$ cm²/s, $\mu_2 = 50$ cm²/s, and a range of h_1 and μ'_1 values, namely: (a) $h_1 = 10$ m, $\mu'_1 = 500$ cm²/s, with a no slip condition; (b) $h_1 = 10$ m, $\mu'_1 = 50$ cm²/s, with a no slip condition; (c) $h_1 = 40$ m, $\mu'_1 = 50$ cm²/s, with a no slip condition; (d) $h_1 = 40$ m, $\mu'_1 = 50$ cm²/s, with a slip condition.

evident that in the case in which $\mu'_1 = 50$ cm²/s, a high shear region occurs at the level of the thermocline. When $\mu'_1 = 500$ cm²/s this high shear region is significantly reduced, as is to be expected from a comparison of the vertical structure functions shown in Fig. 4. When h_1 is increased to 40 m, it is evident from Fig. 5, profile (c), that the high shear region now occurs at approximately mid-depth, reflecting the vertical structure of the modes shown in Fig. 4(c).

It is interesting to note that the u component of current, the current at right angles to the wind direction, exhibits a simple vertical variation, the major features of which can be represented by a linear combination of the first two modes. The v component of current in the case of $h' = 10$ m shows a near constant value above the thermocline, with a return flow beneath it. A similar vertical structure namely a constant value above the thermocline is shown in the modes. However when $h' = 40$ m, the v component does reverse above the thermocline, reflecting the reversal in sign above the thermocline of the modes computed with $h' = 40$ m (see Fig. 4).

Profiles computed with a slip condition were not significantly different from those shown in Fig. 5(a), (b), (c). This is to be expected since it is friction at the level of the thermocline (i.e. the magnitude of μ'_1) that is important, and not bottom friction. In essence the thermocline prevents the wind's energy from reaching the sea bed.

It is interesting to note the significant difference in the magnitude of the surface current computed with $h' = 10$ m, compared with that computed with $h' = 40$ m. This is because in a strongly stratified sea, the wind's energy only acts upon the mixed layer of depth h'. The wind's momentum is spread over this layer, and consequently the thicker this layer, the lower the surface current. In weaker stratified conditions, the problem is more complex. This case is currently being investigated and a discussion is beyond the scope of this paper.

The "slab like" behaviour of surface current above the thermocline has been observed in near surface current measurements taken during storm wind conditions. A recent excellent review of observational evidence is given in Gordon (1982b).

4. Concluding remarks

By using the Galerkin method in the vertical, the solution of the three dimensional hydrodynamic equations describing motion in a finite depth sea region has been developed in terms of an expansion of vertical structure functions (modes). Both slip and no-slip bottom

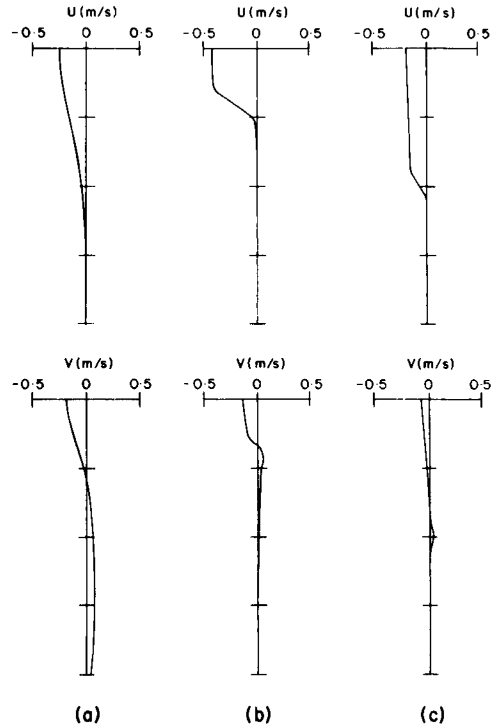

Fig. 5. Steady state u and v components of drift current computed with a wind stress $\tau_x = 0.0$, $\tau_y = -10$ dP_a using the viscosity profile given in Fig. 1(e), with $h'_3 = 2$ m, $h_3 = 6$ m, $h_2 = 10$ m, $\mu_0 = 5000$ cm^2/s, $\mu_1 = 1000$ cm^2/s, $\mu_2 = 50$ cm^2/s, and a range of h_1 and μ'_1 values, namely: (a) $h_1 = 10$ m, $\mu'_1 = 500$ cm^2/s; (b) $h_1 = 10$ m, $\mu'_1 = 50$ cm^2/s; (c) $h_1 = 40$ m, $\mu'_1 = 50$ cm^2/s. A no slip bottom boundary condition was used.

boundary conditions can be incorporated in the method.

Vertical structure functions for arbitrary vertical variations of eddy viscosity can be accurately computed using either B-splines or the Runge-Kutta-Merson method. When B-splines are used it is necessary to ensure that there is a high resolution of knots and hence splines in regions where there is significant vertical variation in the vertical modes. In the case of wind driven motion in a homogeneous sea, enhanced resolution is required in the near surface and near bed regions. In a stratified sea, enhanced resolution is required at the level of the thermocline.

An alternative to using spline functions to compute the modes is to apply the Runge-Kutta-Merson method. Although this is computationally more time consuming, the fact that the accuracy of the method can be checked, and the grid step automatically refined to maintain accuracy in regions where the methods change very rapidly, makes this a convenient method of computing the modes and their associated integrals. The calculations presented here showed that, both methods were accurate and consequently the application of either the spline method or Runge-Kutta-Merson method of computing the modes is not important. However since the majority of computer mathematical libraries contain the Runge Kutta method, with error checking, this approach may in practice be simpler to implement.

The solution of the linear hydrodynamic equations using an expansion of modes in essence yields a system of uncouple equations which is computationally very economical to integrate (Davies and Stephens, 1983). In practice an expansion of the order of ten modes yields an accurate solution, although this number of terms may have to be increased in deep water (Davies, 1984a).

The method is sufficiently general to deal with sea regions of arbitrary extent (see Davies and Furnes, 1980) and by using the Galerkin method, buoyancy effects can be included in stratified sea regions (Davies, 1981). The approach is flexible enough to accommodate time and horizontally varying viscosity, which may in practice be related directly to the current (see Davies, 1981; Davies and Furnes, 1980).

Calculations are presently in progress using the methods developed in this paper, to examine the time variation of current profiles following the sudden imposition of a wind field upon a sea area initially at rest. The influence of setup against coastlines, bottom friction (Davies, 1985), and mixed layer depth upon current profiles is also being examined, and the results will be reported in due course.

5. Acknowledgements

The authors are indebted to Dr. N. S. Heaps and Mr. A. Evjen for a number of useful comments on this work. The care taken by Mr. R. A. Smith in preparing diagrams and Mrs. P. Lynch and Mrs. L. Parry in typing the manuscript is appreciated.

6. Appendix

For larger r, the eigenvalues can be estimated from

$$\tilde{\varepsilon}_r = [(r - \mathscr{H})\,\delta]^2 \tag{A1}$$

where $\tilde{\varepsilon}_r$ denotes the estimated eigenvalues, $\delta = \pi / \int_0^1 \psi^{-1/2} \mathrm{d}\sigma$, and $\mathscr{H}$ is some quantity between 0 and 1 depending on the form of the boundary conditions of the eigenvalue equation (2.12). The formula can be derived by using the WKB method as in Murray (1974), ch 6.2 where formula (6.55) is directly applicable to our equation after a change of variables.

Thus, let $\mathrm{d}\sigma = \psi\,\mathrm{d}x$ then (2.7) becomes

$$\frac{d^2 f}{\mathrm{d}x^2} + \varepsilon\psi f = 0. \tag{A2}$$

Then the asymptotic solution for large $\sqrt{\varepsilon}$ is

$$f(\sigma) = \psi^{-1/4} \exp \times \left\{ \pm i\sqrt{\varepsilon} \int_\sigma \psi^{-1/2} \mathrm{d}\sigma' + \mathrm{O}\left(\frac{1}{\sqrt{\varepsilon}}\right) \right\}. \tag{A3}$$

If, for example, $f_r = 0$ at $\sigma = 0$ and $\sigma = 1$ we have the condition that,

$$\sqrt{\varepsilon_r} \int_0^1 \psi^{-1/2} \mathrm{d}\sigma' + \mathrm{O}\left(\frac{1}{\sqrt{\varepsilon_r}}\right) = r\pi, \tag{A4}$$

with r giving the number of half-periods of oscillation of the eigenfunction between $\sigma = 0$ and $\sigma = 1$. If the boundary conditions are different, for example $f_r' = 0$ for $\sigma = 0$ and $f_r = 0$ for $\sigma = 1$ then r must be replaced by $r - \frac{1}{2}$.

From (A4) we obtain that

$$\sqrt{\varepsilon_r} = \frac{r\pi}{\int_0^1 \psi^{-1/2} \mathrm{d}\sigma'} + \mathrm{O}\left(\frac{1}{r}\right) \tag{A5}$$

and hence

$$\varepsilon_r = \left(\frac{r\pi}{\int_0^1 \psi^{-1/2} \mathrm{d}\sigma'} \right)^2 + \mathrm{O}(1). \tag{A6}$$

This asymptotic formula is quite accurate for large r.

Eq. (A6) can also be derived in a much simpler manner. If ε is large, then f becomes a rapidly oscillating function of σ. If $\psi(\sigma)$ is approximated by a constant value, then in a small region between σ and $\mathrm{d}\sigma$, then eq. (2.7) becomes

$$\frac{\mathrm{d}^2 f}{\mathrm{d}\sigma^2} + \frac{\varepsilon}{\psi} f = 0. \tag{A7}$$

The solution of (A7) will be proportional to $\sin(\sqrt{\varepsilon/\psi}\,\sigma + \text{phase})$, and the number of oscillation within this region will be approximately

$$\sqrt{\frac{\varepsilon}{\psi}} \frac{\mathrm{d}\sigma}{2\pi}.$$

The number of oscillations over the range $0 \leqslant \sigma \leqslant 1$ will be approximately,

$$\int_0^1 \sqrt{\frac{\varepsilon}{\psi}} \frac{\mathrm{d}\sigma}{2\pi}.$$

If the boundary conditions are $f = 0$ for $\sigma = 0$ and $\sigma = 1$ then the number of oscillations must be $\frac{1}{2}$, $\frac{2}{2}$, $\frac{3}{2}$, etc. for the first, second, etc. eigenfunctions. Thus for large r the eigenvalues can be estimated by

$$\int_0^1 \sqrt{\frac{\varepsilon}{\psi}} \frac{\mathrm{d}\sigma}{2\pi} = \frac{r}{2}. \tag{A8}$$

Rearranging (A8), gives

$$\varepsilon_r = \left(\frac{r\pi}{\int_0^1 \psi^{-1/2} \mathrm{d}\sigma} \right)^2 \tag{A9}$$

a significantly simpler derivation of (A6) than that first described.

REFERENCES

Baker, J. R. and Jordan, T. F. 1980. Vertical-structure functions for time-dependent flow in a well-mixed fluid with turbulent boundary layers at the bottom and top. *J. Phys. Oceanogr. 10*, 1691–1694.

Baker, J. R. and Jordan, T. F. 1981. Vertical structure of time-dependent flow for viscosity that depends on both depth and time. *J. Phys. Oceanogr. 11*, 1673–1674.

Bowden, K. F., Fairbairn, L. A. and Hughes, P. 1959. The distribution of shearing stresses in a tidal current. *Geophys. J. R. Astron. Soc. 2*, 288–305.

Bowden, K. F. 1978. Physical problems of the benthic boundary layer, *Geophys. Surv. 3*, 255–296.

Carter, D. J. T. 1982. Prediction of wave height and period for a constant wind velocity using the JONSWAP results. *Ocean Eng. 9*, 17–33.

Channon, R. D. and Hamilton, D. 1971. Sea Bottom velocity profiles on the Continental Shelf south-west of England. *Nature 231*, 383–385.

Cooper, C. K. and Pearce, B. 1982. Numerical simulations of hurricane-generated currents. *J. Phys. Oceanogr. 12*, 1071–1091.

Davies, A. M. 1980. Application of the Galerkin method to the formulation of a three-dimensional non-linear hydrodynamic sea model. *Appl. Math. Modelling 4*, 245–256.

Davies, A. M. 1981. Three-dimensional hydrodynamic models. Part 1. A homogeneous ocean-shelf model. Part 2. A stratified model of the northern North Sea pp. 370–426 in Vol. 2. *The Norwegian Coastal Current* (eds. R. Saetre and M. Mork). Bergen University 795 pp.

Davies, A. M. 1983a. Formulation of a linear three-dimensional hydrodynamic sea model using a Galerkin-eigenfunction method. *Int. J. Numer. Methods in Fluids 3*, 33–60.

Davies, A. M. 1983b. Application of a Galerkin-eigenfunction method to computing currents in homogeneous and stratified seas, pp. 287–301. In *Numerical methods for fluid dynamics*, eds. Morton, K. W. and Baines, M. J. Academic Press, London.

Davies, A. M. 1985. A three-dimensional modal model of wind induced flow in a sea region. *Prog. Oceanogr. 15*, 71–128.

Davies, A. M. 1986. Spectral models in continental shelf oceanography, to appear in: SCOR book on *Coastal oceanography*, ed. Heaps, N. S.,

Davies, A. M. and Owen, A. 1979. Three-dimensional numerical sea model using the Galerkin method with a polynomial basis set. *Appl. Math. Modelling 3*, 421–428.

Davies, A. M. and Furnes, G. K. 1980. Observed and computed M_2 tidal currents in the North Sea. *J. Phys. Oceanogr. 10*, 237–257.

Davies, A. M. and Stephens, C. V. 1983. Comparison of the finite difference and Galerkin methods as applied to the solution of the hydrodynamic equations. *Appl. Math. Modelling 7*, 226–240.

Furnes, G. K. 1983. A three-dimensional numerical sea model with eddy viscosity varying piecewise linearly in the vertical. *Cont. Shelf Res. 2*, 231–241.

Gjevik, B. and Røed, L. P. 1976. Storm surges along the western coast of Norway. *Tellus 28*, 166–182.

Gordon, R. B. 1982a. Wind driven circulation in Narragansett Bay, Ph.D. Thesis. University of Rhode Island.

Gordon, R. L. 1982b. Coastal ocean current response to storm winds. *J. Geophys. Res. 87*, 1939–1951.

Hall, G. and Watt, J. M. 1976. *Modern numerical methods for ordinary differential equations*. Clarendon Press, Oxford.

Hamming, R. W. 1962. *Numerical methods for scientists and engineers*. McGraw-Hill Book Company, pp. 411.

Heaps, N. S. 1972. On the numerical solution of the three-dimensional hydrodynamical equations for tides and storm surges. *Mem. Soc. R. Sci. Liege, Belgium. Ser 6 2*, 143–180.

Heaps, N. S. 1981. Three-dimensional model for tides and surges with vertical eddy viscosity prescribed in two layers—1. Mathematical formulation. *Geophys. J. R. Astron. Soc. 64*, 291–302.

Ichiye, T. 1967. Upper ocean boundary-layer flow determined by dye diffusion. *Phys. Fluids. Suppl. 10*, 270–277.

Koutitas, C. 1978. Numerical solution of the complete equations for nearly horizontal flows. *Adv. Water Resour. 1*, 213–217.

Mortimer, C. H. 1952. Water movements in lakes during summer stratification; evidence from the distribution of temperature in Windermere. *Phil. Trans. B236*, 355–404.

Mork, M. 1972. On the time-dependent motion generated by wind an atmospheric pressure in a continuously stratified ocean of varying depth. Geophys. Inst, Div A., Phys. Oceanogr., University of Bergen, Norway.

Murray, J. D. 1974. *Asymptotic analysis*. Oxford University Press.

Neumann, G. and Pierson, W. J. 1964. *Principles of physical oceanography*. Prentice-Hall.

Nihoul, J. C. J. 1977. Three-dimensional model of tides and storm surges in the shallow well-mixed continental sea. *Dyn. Atmos. Ocean. 2*, 29–47.

Røed, L. P. 1979. Storm surges in stratified seas. *Tellus 31*, 330–339.

Smith, T. J. 1982. On the representation of Reynolds stress in estuaries and shallow coastal sea. *J. Phys. Oceanogr. 12*, 914–921.

Weber, J. E. 1981. Ekman Currents and mixing due to surface gravity waves. *J. Phys. Oceanogr. 11*, 1431–1435.

Wolf, J. 1980. Estimation of shearing stresses in a tidal current with application to the Irish Sea. In *Marine turbulence*, ed. Nihoul, J. C. J. Elsevier Scientific Publishing Company, Amsterdam.